HHS Public Access

Author manuscript

Nat Med. Author manuscript; available in PMC 2018 February 14.

Published in final edited form as:

Nat Med. 2017 September ; 23(9): 1055–1062. doi:10.1038/nm.4379.

Intrinsic BET inhibitor resistance in prostate cancer caused by SPOP mutation-mediated BET protein stabilization

Pingzhao Zhang[1,6,13], **Dejie Wang**[2,3,13], **Yu Zhao**[2,13], **Shancheng Ren**[7,13], **Kun Gao**[1,13], **Zhenqing Ye**[8], **Shangqian Wang**[9], **Chun-Wu Pan**[2], **Yasheng Zhu**[7], **Yuqian Yan**[2], **Yinhui Yang**[2], **Di Wu**[2], **Yundong He**[2], **Jun Zhang**[10], **Daru Lu**[1], **Xiuping Liu**[11], **Long Yu**[1], **Shimin Zhao**[1], **Yao Li**[1], **Dong Lin**[12], **Yuzhuo Wang**[12], **Liguo Wang**[8], **Yu Chen**[9], **Yinghao Sun**[7,*], **Chenji Wang**[1,*], and **Haojie Huang**[2,4,5,*]

[1]State Key Laboratory of Genetic Engineering, Collaborative Innovation Center for Genetics and Development, School of Life Sciences, Fudan University, Shanghai 200433, China

[2]Department of Biochemistry and Molecular Biology, Mayo Clinic College of Medicine, Rochester, MN 55905, USA

[3]Department of Gastroenterology, Jiangxi Institute of Gastroenterology and Hepatology, The First Affiliated Hospital of Nanchang University, Nanchang, Jiangxi 330006, China

[4]Department of Urology, Mayo Clinic College of Medicine, Rochester, MN 55905, USA

[5]Mayo Clinic Cancer Center, Mayo Clinic College of Medicine, Rochester, MN 55905, USA

[6]Shanghai Cancer Center, Institute of Biomedical Sciences, Shanghai Medical College of Fudan University, Shanghai 200032, China

[7]Department of Urology, Shanghai Changhai Hospital, Second Military Medical University, Shanghai 200433, China

[8]Division of Biomedical Statistics and Informatics, Mayo Clinic College of Medicine, Rochester, MN 55905, USA

[9]Human Oncology and Pathogenesis Program, Memorial Sloan-Kettering Cancer Center, New York, NY 10065, USA

[10]Department of Laboratory Medicine and Pathology, Mayo Clinic College of Medicine, Rochester, MN 55905, USA

[*]Correspondence should be addressed to: Haojie Huang (huang.haojie@mayo.edu); Chenji Wang (chenjiwang@fudan.edu.cn); Yinghao Sun (sunyhsmmu@126.com).

[13]These authors contributed equally to this work.

Contribution of Authors

HH and CW conceived the study. P.Z., D.W., Y.(Yu)Z., S.R., K.G., Z.Y., S.W., C.-W.P., Y.Z., Y.Y., D.(Di)W., Y.H., D.L., L.Y., S.Z., Y.L., D.(Dong)L., Y.W., Y.C. acquired patient samples, generated organoids and performed the experiments and data analysis. Z.Y. and L.W. performed bioinformatics analysis. X.L. and J.Z. supervised histological and IHC data analysis. H.H., C.W. and Y.S. wrote the paper.

Competing Financial Interests Statement

The authors declare no competing financial interests.

[11]Department of Pathology, School of Basic Medical Sciences, Shanghai Medical College of Fudan University, Shanghai 200032, China

[12]Department of Experimental Therapeutics, BC Cancer Research Centre, Vancouver, BC V5Z 1L3, Canada

Abstract

Bromodomain and extraterminal domain (BET) protein inhibitors are emerging as promising anti-cancer therapies. The gene encoding the E3 ubiquitin ligase substrate-binding adaptor speckle-type POZ protein (SPOP) is most frequently mutated in prostate cancer. Here we demonstrate that wild-type SPOP binds to and induces ubiquitination and proteasomal degradation of BET proteins (BRD2, BRD3 and BRD4) by recognizing a common degron motif. In contrast, prostate cancer-associated SPOP mutants impair binding and proteasomal degradation of BET proteins, thus inducing their accumulation in prostate cancer cells and patient specimens. Transcriptome and BRD4 cistrome analyses reveal that SPOP mutation enhances BRD4-dependent expression of GTPase RAC1 and cholesterol biosynthesis genes and AKT-mTORC1 activation. SPOP mutant expression confers BET inhibitor resistance and this effect can be overcome by AKT inhibitors. Thus, SPOP mutations promote AKT-mTORC1 activation and intrinsic BET inhibitor resistance by stabilizing BET proteins, suggesting that SPOP mutation can be an effective biomarker to guide BET inhibitor-oriented therapy of prostate cancer.

Ubiquitously-expressed BET proteins including BRD2, BRD3 and BRD4 function as key factors for transcriptional activation of distinct sets of cancer-related genes through context-specific interaction with acetylated histones and/or transcription factors[1,2]. Several small molecule inhibitors specifically targeting the bromodomains of BET proteins have been developed and display promising anti-cancer activity via selective blockage of expression of cancer promoters such as MYC in multiple myeloma and androgen receptor (AR) in prostate cancer[1–6]. While BET inhibitors are undergoing clinical trials for treatment of various cancer types, several mechanisms of drug resistance have been documented[7–9]. At present, there is no genetic alteration(s) can be exploited as a biomarker to guide targeted use of these drugs.

SPOP is the substrate recognition subunit of the CULLIN3-RBX1 E3 ubiquitin ligase (CRL) complex. SPOP binding triggers the ubiquitination and proteasomal degradation of target proteins mediated by RBX1-dependent recruitment of E2 ubiquitin-conjugating enzyme into the CRL complex. Cancer whole genome- and exome-sequencing studies reveal that *SPOP* is the most frequently mutated gene in primary prostate cancer[10,11]. Notably, SPOP mutations detected in prostate cancer occur in the structurally defined substrate-binding motif termed MATH domain[10,12–14], suggesting that the pathophysiology of SPOP mutations is likely mediated by impaired ubiquitination of substrates.

To identify new degradation substrates of SPOP, we performed yeast two-hybrid screens using the full-length SPOP as bait. A total of 246 positive clones were obtained, including known SPOP substrates DEK and SRC-3 (Supplementary Table 1). Gene Ontology analysis showed that SPOP bound to a number of proteins involved in regulation of various signaling pathways, but the top hit was BET proteins (Fig. 1a and Supplementary Table 2). Co-

immunoprecipitation (co-IP) assays confirmed that ectopically expressed and endogenous SPOP and BRD2/3/4 proteins interacted with each other in 293T and LNCaP prostate cancer cells (Fig. 1b and Supplementary Fig. 1a). Thus, SPOP interacts with BET proteins in physiological conditions.

BET proteins play key roles in epigenetic regulation and cancer, but little is known about their post-translational modifications and downstream functions. Treatment of LNCaP cells with proteasome inhibitors Bortezomib and MG132 inevitably increased BRD2/3/4 protein, but not mRNA expression (Supplementary Fig. 1b, c). MLN4924, a small molecule inhibitor of NEDD8-activating enzyme that is required for activation of CRLs, also caused accumulation of BRD2/3/4 at protein level (Supplementary Fig. 1b, c). Expression of wild-type SPOP markedly decreased BRD2/3/4 proteins, and this effect was completely reversed by MG132 treatment (Fig. 1c). Knockdown of SPOP increased the steady-state level of endogenous BRD2/3/4 protein and prolonged the protein half-life while had no overt effect on mRNA expression in LNCaP cells (Fig. 1d and Supplementary Fig. 1d–f). Similar results were obtained in 22Rv1 and BPH-1 prostatic cell lines (Fig. 1d). Moreover, only wild-type SPOP, but not substrate binding- and CUL3 binding-deficient mutants (ΔMATH and ΔBTB, respectively) degraded BRD2/3/4 proteins (Supplementary Fig. 1g). Wild-type SPOP induced K48-dependent polyubiquitination of these proteins in cells and this effect relied on its enzymatic activity (Fig. 1e and Supplementary Fig. 1h–i). We further showed that the SPOP-CULLIN3-RBX1 complex catalyzed BRD4 ubiquitination in vitro (Fig. 1f). Thus, functioning as a CRL substrate-binding adaptor, SPOP promotes ubiquitination and proteasomal degradation of BRD2/3/4 proteins in prostate cancer cells.

Substrate-binding consensus (SBC) motifs (Φ-π-S/T-S/T-S/T where Φ is a nonpolar residue and π is a polar residue[15]) have been well characterized in known SPOP substrates such as MacroH2A and DEK[12]. We found the existence of a perfectly matched SBC motif in the region between bromodomain-1 (BD1) and BD2 in BRD2/3/4 proteins (Fig. 2a, b), which also localizes within the minimal SPOP-interaction region defined by yeast two-hybrid clones of BRD2/3/4 (Fig. 1a). Co-IP assays revealed that deletion of the putative SBC motif in BRD2/3/4 not only abolished SPOP binding and SPOP-mediated ubiquitination and degradation of BRD2/3/4, but also significantly prolonged the half-life of these proteins (Fig. 2b–g). Thus, we identified a common, functionally conserved SBC motif in BRD2/3/4 proteins that is required for SPOP-dependent ubiquitination and degradation.

Because SPOP mutations in prostate cancers occur in the MATH domain that is responsible for substrate binding[16], we hypothesized that prostate cancer-associated mutations impair the ability of SPOP to degrade BRD2/3/4. We generated 11 prostate cancer-associated SPOP mutants. Co-IP assays demonstrated that the BRD2/3/4-binding ability of all 11 SPOP mutants was largely impaired compared with wild-type SPOP (Fig. 3a and Supplementary Fig. 2a). SPOP-mediated ubiquitination of these proteins was also markedly attenuated by these mutations (Fig. 3b and Supplementary Fig. 2b). SPOP mutants failed to degrade, but rather elevated endogenous BRD2/3/4 protein levels, a dominant-negative effect similarly occurred to known SPOP substrates such as DEK, ERG and SRC-3[12–14] (Fig. 3c). Thus, prostate cancer-associated SPOP mutants result in the stabilization of BRD2/3/4 proteins in prostate cancer cells.

To examine the effect of SPOP mutations on BET protein levels in patient specimens, we analyzed BRD2/3/4 protein levels in two cohorts constituting 99 primary prostate tumors (Supplementary Table 3). We identified 13 SPOP-mutated tumors through whole-genome sequencing and/or Sanger sequencing. The SPOP mutation frequency in our samples is consistent with the previous findings in different cohorts of prostate cancer[10,11]. Immunohistochemistry (IHC) showed that approximately 85%, 92% and 85% of SPOP-mutated tumors exhibited strong or intermediate straining of BRD2, BRD3 and BRD4 proteins, respectively (Fig. 3d, e). In contrast, only 40% or less of SPOP-WT tumors exhibited strong or intermediate straining whereas majority of them (approximately 71%, 66% and 59% for BRD2, BRD3 and BRD4, respectively) exhibited weak staining (Fig. 3d, e). *BRD2/3/4* mRNA expression was relative lower in SPOP-mutated tumors than that in SPOP-WT specimens in our cohorts, although the difference did not reach statistical significance (except *BRD2*) (Supplementary Fig. 2c). A similar trend was observed in The Cancer Genome Atlas (TCGA) dataset (Supplementary Fig. 2d). These findings indicate that BRD2/3/4 protein levels were elevated in SPOP-mutated prostate cancer specimens and this was unlikely caused by increases in mRNA level.

Small molecule inhibitors of BET proteins are being actively tested as promising epigenetic-targeted therapeutics of cancer[1,3–9,17,18]. We examined if SPOP-mediated degradation of BET proteins influences the anti-cancer efficacy of BET inhibitors in prostate cancer cells. Knockdown of endogenous SPOP by small hairpin RNAs (shRNAs) not only increased BRD2/3/4 protein expression, but also enhanced proliferation in C4-2 cells and this effect was abolished by co-knockdown of BRD2/3/4 proteins (Supplementary Fig. 3a–g). Consistent with a previous report[6], we demonstrated that the BET inhibitor JQ1 robustly inhibited prostate cancer cell growth, but this effect was largely attenuated in SPOP-knockdown cells (Supplementary Fig. 3a–c). SPOP depletion-mediated JQ1 resistance was reversed by knockdown of BRD4 alone (Supplementary Fig. 3h–j). However, BRD4 knockout cells became highly resistant to JQ1 when BRD2/3 were largely depleted (Supplementary Figure 3k, l). This result is not surprising since little or no druggable targets (BRD2/3/4 proteins) were present in these cells. These data suggest that protein levels of BRD2/3/4 may represent a molecular determinant for JQ1 sensitivity in SPOP-deficient prostate cancer cells.

Phenylalanine 133 (F133) is the most frequently mutated residue in SPOP[10]. To recapitulate the situation in patients, we introduced SPOP-F133V mutant into SPOP-WT-expressing C4-2 and 22Rv1 cells. Expression of SPOP-F133V not only induced accumulation of BRD2/3/4 proteins, but also caused a significant increase in proliferation in both cell lines (Supplementary Fig. 3m, n). While JQ1 treatment inhibited growth of empty vector (EV)-expressing C4-2 and 22Rv1 cells, the effect of JQ1 was largely impeded in SPOP-F133V-expressing cells (Supplementary Fig. 3n). SPOP-F133V expression also caused similar resistance to another BET inhibitor i-BET in C4-2 and 22Rv1 cells (Supplementary Fig. 3o–q). We further showed that SPOP-F133V mutant conferred JQ1-resistance in C4-2 xenograft tumors in mice (Fig. 4a–c). SPOP-F133V-mediated JQ1-resistance was completely reversed by co-depletion of BRD2/3/4 proteins in C4-2 cells in vitro and in C4-2 xenografts in mice (Fig. 4a–c and Supplementary Fig. 4a–c). SPOP-F133V expression also induced accumulation of known SPOP substrates ERG, DEK and SRC-3[12–14] in C4-2 and 22Rv1

cells and C4-2 tumors in mice (Supplementary Fig. 3m and 4d). However, JQ1 treatment largely decreased ERG expression (Supplementary Fig. 3m and 4d, e), which is consistent with similar findings in acute myeloid leukemia cells[19]. Knockdown of ERG by shRNAs had no overt effect on SPOP-F133V-mediated JQ1 resistance in C4-2 cells, and similar results were obtained in DEK-knockdown cells (Supplementary Fig. 4e, f). SRC-3 knockdown slightly sensitized SPOP-F133V cells to JQ1, but the effect was not statistically significant (Supplementary Fig. 4e, f). Thus, our data suggest SPOP mutation-conferred BET inhibitor resistance is largely mediated by elevation of BRD2/3/4 proteins in prostate cancer cells.

Next, we investigated the role of SPOP mutation-induced accumulation of BRD proteins in BET inhibitor resistance in clinically-oriented models. Among three prostate cancer patient-derived organoid lines examined, one harbors a W131R mutation in SPOP. W131 belongs to a conserved residue in the substrate-binding cleft[10]. We demonstrated that W131R mutation was deficient in binding to and mediating ubiquitination and degradation of BRD4 (Supplementary Figure 5a–c). Most importantly, the W131R-expressing organoid expressed more BRD2/3/4 proteins and was resistant to JQ1 compared to two SPOP WT counterparts under both 2D and 3D growth conditions (Supplementary Figure 5d–g). These data indicate that SPOP mutation confers BET inhibitor resistance in patient-derived primary cultures.

It is worth noting that BET inhibitors have been shown to induce BRD4 accumulation in different cell types, but the underlying mechanism is unclear[6,20]. We demonstrated the effect occurred at post-transcriptional level (Fig. 4a and Supplementary Fig. 3m, 6a, b). We further showed that JQ1 diminished SPOP-BRD2/3/4 protein interaction, partially blocked SPOP-induced BRD2/3/4 ubiquitination and degradation, and prolonged protein half-life even in SPOP-F133V-expressing cells (Supplementary Fig. 6c–h). Thus, while inhibiting their activities, BET inhibitors undesirably disturb BET protein proteolysis and this effect appears to be mediated by SPOP-dependent and -independent mechanisms.

To define the signaling pathways that mediate BET inhibitor resistance in SPOP-mutated cells, we performed transcriptome analysis in control (EV) and SPOP-F133V-expressing C4-2 cells treated with or without JQ1. Through unsupervised cluster analysis we identified 5,079 JQ1-downregulated genes in both control and SPOP-F133V cells, including *MYC* and *AR*, two known targets of BET inhibitors[3,5,6] (Supplementary Fig. 7a). Previous studies suggest that MYC may not be the major anti-cancer target of JQ1 in prostate cancer cells[6]. In agreement with this report, we found that JQ1 treatment markedly decreased MYC protein expression, which is consistent with substantial reduction of BRD4 binding in the *MYC* gene enhancer in both JQ1-sensitive (control) and -resistant (SPOP-F133V) C4-2 cells (Supplementary Fig. 7b–d). JQ1 also largely decreased AR protein level, BRD4 binding in the *AR* gene promoter and AR transcriptional activity in both control and SPOP-F133V cells (Supplementary Fig. 7b–f), and further knockdown of AR by shRNAs did not affect JQ1 sensitivity in these cells (Supplementary Fig. 7g, h). Collectively, these findings suggest that BET inhibitor resistance in SPOP-mutated prostate cancer cells is likely mediated by MYC- and AR-independent pathways.

Further analysis of RNA-seq data revealed 1,017 genes whose expression was suppressed by JQ1 in control cells but remained either unchanged or upregulated in F133V-mutant cells (Fig. 4d). 129 of them were highly upregulated in SPOP-mutated prostate tumors compared to SPOP-WT tumors in the TCGA cohort (Fig. 4e and Supplementary Table 4). Notably, these aberrantly upregulated genes significantly overlapped with the BRD4 target genes commonly identified in C4-2 cells transfected with SPOP-F133V or HA-BRD4 (Fig. 4f and Supplementary Fig. 8a–c). Ingenuity pathway analysis of the overlapped genes indicated that the top hit was the cholesterol biosynthesis pathway and four members of this pathway including *FDFT1*, *DHCR24*, *DHCR7* and *MVD* were upregulated in SPOP-mutated tumors (Fig. 4e, f). Cholesterol-rich lipid rafts have been linked to AKT activation and prostate cancer cell survival[21–23]. Since the RHO GTPase family member RAC1 can also activate the AKT-mTORC1 pathway by directly binding to mTOR[24,25] and RAC1 was upregulated in SPOP-mutated tumors (Fig. 4e), we chose to focus on these two pathways. Meta-analysis also showed BRD4 binding at the RAC1 locus in different cell types (Supplementary Fig. 8d). RNA-seq analysis showed that global transcriptional changes caused by BRD2/3/4 overexpression in C4-2 cells significantly overlapped with the genes associated with JQ1 resistance in F133V-mutant cells, including RAC1 (Supplementary Figure 8e–g and Supplementary Table 5). ChIP-seq and ChIP-qPCR assays showed that BRD4 readily bound at the *RAC1* gene promoter in control cells, but the binding was largely enhanced by expression of SPOP-F133V or HA-BRD4 (Fig. 4f, g and Supplementary Fig. 8c, h). Increased BRD4 binding was unlikely caused by histone acetylation changes since expression of SPOP F133V or BRD proteins had no effect on the level of H3K27ac, H4K5ac and H4K8ac, both globally and in the *RAC1* locus (Supplementary Fig. 8i, j). BRD4-dependent regulation of RAC1 was confirmed by gene knockdown experiments (Supplementary Fig. 8k, l), providing further evidence that *RAC1* is a *bona fide* BRD4 target gene. Additionally, increased BRD4 binding and RAC1 mRNA and protein expression correlated with high levels of BRD4 proteins in JQ1-resistant SPOP-F133V cells compared to JQ1-untreated control cells (Fig. 4g and Supplementary Fig. 8c, m, n). Furthermore, SPOP-F133V expression substantially increased phosphorylation of AKT and S6K, a downstream kinase of mTORC1, in both C4-2 and 22Rv1 cells regardless of JQ1 treatment (Supplementary Fig. 3m, 8o). Knockdown of RAC1 not only inhibited SPOP-F133V-augmented AKT and S6K phosphorylation, but also abolished SPOP-F133V-mediated JQ1 resistance in C4-2 cells (Supplementary Fig. 8o, p).

ChIP-seq and ChIP-qPCR assays showed that BRD4 readily bound in the promoters of cholesterol synthesis genes *FDFT1*, *DHCR24*, *DHCR7* and *MVD* in control cells and the binding was enhanced by SPOP-F133V (Supplementary Fig. 9a–c), and this effect was unlikely caused by global or locus-specific histone acetylation changes (Supplementary Fig. 8i, 9d). Knockdown of BRD4 largely decreased expression of these genes at mRNA and protein levels in both control and SPOP-F133V cells (Supplementary Fig. 8n, 9e). With concomitant induction of BRD4 protein levels, SPOP-F133V upregulated the expression of cholesterol synthesis genes at both mRNA and protein levels and enhanced BRD4 binding in their promoters (Supplementary Fig. 9b, c, e, f). JQ1 treatment largely inhibited expression of these genes and BRD4 binding at their promoters in control cells, but the effect was not pronounced in SPOP-F133V cells (Supplementary Fig. 9b, c, f, g). Co-depletion of these

cholesterol synthesis genes abolished SPOP-F133V-induced activation of the AKT-mTORC1 pathway and JQ1-resistance in C4-2 cells (Supplementary Fig. 9h, i). Similar to SPOP mutant, moderate overexpression of BRD2/3/4 increased cholesterol biosynthesis and AKT/mTORC1 activation (Supplementary Fig. 8e, 9j). These data imply that both RAC1 and cholesterol synthesis pathways are required to mediate SPOP mutation-induced AKT/mTORC1 activation and JQ1 resistance (Supplementary Fig. 9k).

We further demonstrated that the transcription activator protein 1 (AP-1, a dimer of c-JUN and c-FOS) commonly bound to *RAC1* and cholesterol synthesis gene promoters (Supplementary Fig. 9l, m). Although expression of c-JUN and c-FOS was not affected by SPOP mutation, knockdown of both abolished SPOP F133V-induced upregulation of *RAC1* and cholesterol synthesis genes and activation of AKT/mTORC1 without disturbing BRD4 expression (Supplementary Fig. 9n–p). It has been shown recently that AKT/mTORC1 pathway is activated in the prostate of SPOP F133V knock-in mice and this effect is mediated partially by increased SRC-3 expression[26]. We also demonstrated that SRC-3 knockdown only partially decreased SPOP F133V-induced AKT/mTORC1 activation by selectively affecting expression of *RAC1* and the cholesterol synthesis genes and slightly, but did not significantly diminish F133V-mediated JQ1 resistance (Supplementary Fig. 4f, 9p), reinforcing a partial, co-activator role of SRC-3 in SPOP F133V-mediated AKT/mTORC1 activation. In contrast, depletion of BET proteins almost completely abolished F133V-induced AKT/mTORC1 activation, upregulation of *RAC1* and cholesterol synthesis genes and BET inhibitor resistance (Fig. 4a–c and Supplementary Fig. 9p).

It has been shown that PI3K inhibitor treatment induced expression of receptor tyrosine kinases (RTKs) including HER3, IGF1R and INSR, and the induction was mediated by BRD4, but blocked by BET inhibitor[27]. However, BET inhibitor treatment alone had no effect on RTK expression[27]. Similarly, no effect of JQ1 on expression of these proteins was detected in either JQ1-sensitive (control) or -resistant (SPOP-F133V) C4-2 cells (Supplementary Fig. 10a). We further demonstrated that neither mTORC1 activity (S6K phosphorylation) nor JQ1-resistant growth was affected by knockdown of HER3, IGF1R or INSR individually in SPOP F133V expressing C4-2 cells (Supplementary Fig. 10b–d). These data rule out the potential role of these RTKs in F133V-induced AKT activation and JQ1 resistance in these cells. In contrast, knockdown of AKT (AKT1, AKT2 and AKT3), mTOR or Raptor alone abolished JQ1-resistant growth of SPOP F133V-expressing C4-2 cells (Supplementary Fig. 10e–g). Similar results were obtained by treating SPOP-F133V cells with the allosteric AKT inhibitor MK2206 (Supplementary Fig. 10h). Most recently, a first-in-human phase I study has shown that Ipatasertib (GDC-0068), a novel ATP-competitive AKT inhibitor, exhibits effective antitumor efficacy in patients with solid tumors[28]. We demonstrated that GDC-0068 treatment of SPOP mutant expressing cells not only abolished SPOP mutation-induced activation of AKT downstream pathways, but also completely overcame SPOP mutation-conferred resistance to BET inhibitor in C4-2 cells in culture and tumors in mice (Fig. 4h, i and Supplementary Fig. 10i). These findings highlight the significance of AKT inhibition in overcoming BET inhibitor resistance in SPOP-mutated prostate cancer (Supplementary Fig. 10j).

In summary, our findings demonstrate BRD2/3/4 proteins are degradation substrates of SPOP. We uncover that SPOP mutation not only induces accumulation of these proteins, but also confers intrinsic resistance to BET inhibitors in prostate cancer cells, suggesting that besides SPOP mutations, elevation of BET proteins can be a biomarker to predict BET inhibitor resistance in prostate cancer patients. The TCGA data reveal that SPOP-mutated tumors had the highest AR transcriptional activity among all genotypically distinct subsets of prostate cancer[11]. This observation is further supported by other reports that protein levels of AR and its co-regulators such as SRC-3, ERG and TRIM24 are stabilized by SPOP mutants in prostate cancer[13,14,29,30]. These findings stress that aberrant activation of the AR not only represents a key event that contributes to the pathophysiology of SPOP mutations in prostate cancer, but also can be targeted for treatment of SPOP-mutated tumors. Consistent with recent reports that JQ1 blocks SPOP-proficient prostate cancer cell growth by inhibiting AR expression and activity[6,31], we demonstrate that expression of AR and its downstream genes examined was inhibited by JQ1 in both SPOP-WT and SPOP-F133V mutant-expressing cells. Similarly, BET inhibitor treatment also decreased expression and ERG and its downstream targets[19,32], which is consistent with our finding that knockdown of ERG had little or no effect on SPOP mutation-induced resistance to BET inhibitor. These data suggest that intrinsic BET inhibitor resistance develops independently of the elevated AR and ERG signaling in SPOP-mutated prostate cancer cells. It is worth noting that both AR and ERG directly interact with the bromodomain of BRD4 and their interactions are both sensitive to JQ1[6,19,32]. At present, it is unclear why AR and ERG are vulnerable to BET inhibition irrespective of elevated BET proteins in SPOP-mutated cells, and whether or not this is due to their JQ1-sensitive binding of BET proteins (Supplementary Fig. 10j) warrants further investigation. We also show that expression of SPOP-F133V mutant not only increases the basal levels of phosphorylation of AKT-mTORC1 pathway proteins, but also largely impedes JQ1-induced inhibition of their phosphorylation. Accordingly, we uncover that the levels of *RAC1* and cholesterol biosynthesis genes, both of which are required for activation of the AKT-mTORC1 pathway[21,23–25], are upregulated in SPOP-mutated prostate tumors in patients. Therefore, in addition to demonstrating the essential role of elevated BET proteins and activation of the AKT-mTORC1 pathway in the resistance to BET inhibition as a consequence of SPOP mutation in prostate cancer cells (Supplementary Fig. 10j), we also provide evidence that targeting the AKT pathway using novel therapeutic agents such as the novel AKT inhibitor Ipatasertib can be a viable treatment option to overcome BET inhibitor resistance in SPOP-mutated prostate cancer.

ONLINE METHODS

Antibodies and chemicals

The following antibodies were used: SPOP (ab137537; Abcam), SPOP (16750-1-AP; proteintech), BRD2 (A302-583A; Bethyl), BRD2 (ab139690; Abcam), BRD3 (A302-368A; Bethyl), BRD4 (ab128874; Abcam), BRD4 (A301-985A; Bethyl), Myc (9E10; Sigma-Aldrich), Myc (SC-40; Santa Cruz Biotechnology), FLAG (M2; Sigma), HA (MM5-101R; Convance), Actin (AC-74; Sigma-Aldrich), DEK (13962S; Cell Signaling Technology), ERG (SC-352; Santa Cruz Biotechnology), AR (SC-816; Santa Cruz Biotechnology), SRC-3 (611104; BD), phospho-AKT-S473 (9471; Cell Signaling Technology), phospho-

AKT-T308 (9275S; Cell Signaling Technology), AKT (9272; Cell Signaling Technology), phospho-S6K-T389 (9205; Cell Signaling Technology), S6K (9202; Cell Signaling Technology), β-tubulin (T4026; Sigma-Aldrich), RAC1 (23A8; BD), FDFT1 (ab195046; Abcam), DHCR24 (ab137845; Abcam), DHCR7 (ab103296; Abcam), MVD (ab12906; Abcam), HER3 (12708S; Cell Signaling Technology), INSR (ab131238; Abcam), IGF1R (SC-9038; Santa Cruz Biotechnology), mTOR (2972, Cell Signaling Technology), Raptor (24C12, Cell Signaling Technology). MG132 and cycloheximide were purchased from Sigma-Aldrich, MLN4924, Bortezomib and MK2206 were purchased from Selleckchem. JQ1 was kindly provided by Dr. James Bradner and purchased from Sigma-Aldrich. i-BET762 (i-BET) was purchased from MedchemExpress. GDC-0068 was purchased from Calbiochem.

Plasmids and mutagenesis

Expression vectors for SPOP-WT or mutants are described previously[34]. FLAG-BRD2 and BRD3 constructs were obtained from Dr. S.J. Flint (Princeton University). FLAG-BRD4 constructs were obtained from Dr. Tasuku Honjo (Kyoto University). FLAG-BRD2/3/4 mutants were generated by KOD Plus Mutagenesis Kit (TOYOBO) following the manufacturer's instructions. lenticrisprV2 plasmid (#52961).was purchased from Addgene (USA).

Cell culture, transfection and lentivirus infection

LNCaP, 22Rv1 and 293T cells were obtained from the American Type Culture Collection (ATCC). C4-2 cells were purchased from Uro Corporation (Oklahoma City, OK). BPH-1 cells were kindly provided by Dr. Simon Hayward[35]. 293T cells were maintained in DMEM medium with 10% FBS, while LNCaP, C4-2, 22Rv1 and BPH-1 cells were maintained in RPMI medium with 10% FBS. Cells were transiently transfected using Lipofectamine RNAi MAX (for siRNA transfection) or 3000 (for plasmids transfection) (Thermo Fisher Scientific) according to manufacturer's instructions. pTsin-HA-SPOP-F133V mutant expression or pLKO-based gene knocking down lentivirus vectors or lenticrisprV2-BRD4and packing constructs were transfected into 293T cells. Virus supernatant was collected 48 h after transfection. C4-2 and 22Rv1 cells were infected with viral supernatant in the presence of polybrene (8 μg/ml) and were then selected in growth media containing 1.5 μg/ml puromycin. Sequences of gene-specific shRNAs are listed in Extended Data Table 6. All the cell lines used have been tested and authenticated by karyotyping and prostate cancer cell lines have also been authenticated by examining AR expression and SPOP mutation status. Plasmocin (InvivoGen) was added to cell culture media to prevent mycoplasma contamination. Mycoplasma contamination was tested regularly using Lookout Mycoplasma PCR Detection Kit from Sigma-Aldrich.

Organoid cultures and cell viability assay

Organoid cells were kindly provided by Dr. Yu Chen from MSKCC and cultured according to the methodology as described previously[36]. In brief, organoid cells were imbedded in 40 μl Matrigel each drop and cultured in FBS free DMEM/F12 medium supplied with several growth factors. Cell viability assays were conducted by plating 2,000 organoid cells per well of a collagen coated 96-well cell culture plate in 100 ml media with vehicle (DMSO) control

or JQ1 (0.05 ~ 1 μM). Viable cells were counted by using a CellTiter-Glo (Promega) Luminescent Cell Viability Assay Kit.

Prostate cancer patient samples

Treatment-naive prostate cancer and matched benign tissues were collected from the radical prostatectomy series at Shanghai Changhai Hospital, and the institutional review board of the hospital approved the experimental protocols. Haematoxylin and eosin (H&E) slides of frozen and formalin-fixed paraffin-embedded (FFPE) human tumor tissues and matched benign tissues were examined by a general pathologists and a genitourinary pathologist to confirm histological diagnosis, Gleason score and verify the high-density cancer foci (>80%) of the selected tumor tissue. The frozen blocks for DNA/RNA extraction were examined by the pathologists as described above, followed by consecutive ten 10-μm sections of each tumor. These qualified samples were then used for DNA/RNA isolation. FFPE tissues were used for immunohistochemistry (IHC).

Detection of SPOP mutation prostate cancer patient specimens by whole-genome and Sanger sequencing

For whole genome sequencing, DNA was extracted by phenol-chloroform and purified by the ethanol precipitation method from 32 paired tumor and benign frozen patient samples. DNA samples were fragmented in fragmentation buffer using Covaris Ultrasonicator system. The fragmented DNA with average length of 500 bp was subjected to DNA library construction. Libraries were constructed according to Illumina's protocol with DNA samples. High-throughput short-gun sequencing was performed on the IlluminaHiSeq 2000 platform. For DNA sequencing, pair-end reads with length of 90 bp were generated. Raw reads of DNA sequencing were filtered using an in-house pipeline. Clean DNA reads were processed with SAMTools to remove the PCR duplicates and aligned to the human reference genome hg19 with Burrows-Wheeler Aligner (http://bio-bwa.sourceforge.net/). The whole genome sequencing data have been deposited in The European Genome-phenome Archive with the accession # EGAS00001000888.

For Sanger sequencing, DNA was extracted from all 99 cases of FFPE prostate cancer tissues using a QIAamp DNA FFPE Tissue kit. PCR was performed and PCR products were purified using a GeneJET Extraction kit according to manufacturer's instruction and used for Sanger sequencing. The primers used for DNA amplification were: Amp-Exon6-Forward 5′-ACCCATAGCTTTGGTTTCTTCTCCC-3′; Amp-Exon6-Reverse 5′-TATCTGTTT TGGACAGGTGTTTGCG-3′; Amp-Exon7-Forward 5′-ACTCATCAGATCTGGGAACTGC-3′; Amp-Exon7-Reverse 5′-AGTTGTGGCTTTGATCTGGTT-3′. Amp-Exon6-Reverse and Amp-Exon7-Forward were also used for Sanger sequencing.

Yeast two-hybrid screen

Yeast two-hybrid screen was performed with the full-length SPOP cloned in-frame with the GAL4 DNA binding domain in vector PGBKT7 (Clontech). The yeast cells were transformed with PGBKT7-SPOP and the human fetal brain cDNA library. A total of 2×10^7 independent clones were screened by growth in deficient medium and X-gal staining.

The positive clones were subsequently retested in fresh yeast cells, and the identities of prey were determined with interaction sequence tags (ISTs) obtained by DNA sequencing. The reading frame was verified.

RNA interference

Non-specific control siRNA and gene-specific siRNAs for human SPOP and BRD4 were purchased from Thermo Fisher Scientific Dharmacon. siRNA transfection of cells was performed following the manufacturer's instructions. The sequences of siRNA oligos are: siSPOP#1 5′-GGAUGAUGUAAAUGAGCAA-3′; siSPOP#2 5′-GGACAGCGACTCTGAATCT-3′; siBRD4#1 5′-GAACCUCCCUGAUUACUAU-3′; siBRD4#2 5′-AGCUGAACCUCCCUGAUUA-3′; non-specific control siRNA (siC) 5′-ACAGACUUCGGAGUACCUG-3′.

Co-immunoprecipitation (Co-IP)

To immunoprecipitate the ectopically expressed FLAG-tagged proteins, transfected cells were lysed 24 h post-transfection in BC100 buffer. The whole-cell lysates were immunoprecipitated with the monoclonal anti-FLAG antibody-conjugated M2 agarose beads (Sigma-Aldrich) at 4°C overnight. After three washes with lysis buffer, followed by two washes with BC100 buffer, the bound proteins were eluted using FLAG-Peptide (Sigma-Aldrich) prepared in BC100 for 3 h at 4°C. The eluted protein sample was resolved by SDS-PAGE. To immunoprecipitate the endogenous proteins, cells were lysed with 1× cell lysis buffer (Cell Signaling Technology), and the lysate was centrifuged. The supernatant was precleared with protein A/G beads (Sigma-Aldrich) and incubated with indicated antibody and protein A/G beads at 4°C overnight. Beads were washed five times with lysis buffer and resuspended in sample buffer and analyzed by SDS-PAGE.

Western blot

Cell lysates or immunoprecipitates were subjected to SDS-PAGE and proteins were transferred to nitrocellulose membranes (GE Healthcare Sciences). The membranes were blocked in Tris-buffered saline (TBS, pH 7.4) containing 5% non-fat milk and 0.1% Tween-20, washed twice in TBS containing 0.1% Tween-20, and incubated with primary antibody overnight at 4°C, followed by secondary antibody for 1 h at room temperature. The proteins of interest were visualized using ECL chemiluminescence system (Santa Cruz Biotechnology). Densitometry analysis of protein bands was analyzed on the Gel-Pro Analyzer software.

In vitro ubiquitination assay

In vitro ubiquitination assay was carried out using a protocol reported previously[1]. Briefly, 2 μg APP-BP1/Uba3, 2 μg His-UBE2M enzymes and 5 μg NEDD8 were incubated at 30°C for 2 h in the presence of ATP. The thioester loaded His-UBE2M-NEDD8 was further incubated with 3 μg His-DCNL2, 6 μg CUL3/RBX1 at 4°C for 2 h to obtain the NEDDylated CUL3/RBX1. The NEDDylated CUL3/RBX1, 5 μg GST-SPOP, 5 μg Ub, 500 ng E1, 750 ng E2 (UbcH5a and UbcH5b), and 5 μg His-BRD4-N (amino acids 1–500) were incubated with 0.6 μl 100 mM ATP, 1.5 μl 20 μM ubiquitin aldehyde, 3 μl 10 × ubiquitin

reaction buffer (500 mM Tris-HCl (pH7.5), 50 mM KCl, 50 mM NaF, 50 mM MgCl2 and 5 mM DTT), 3 μl 10 × energy regeneration mix (200 mM creatine phosphate and 2 μg/μl creatine phosphokinase), 3 μl 10 × protease inhibitor cocktail at 30°C for 2 h, followed by western blot analysis. The Ub, E1, E2 and CUL3/RBX1 were purchased from UBIQUIGENT.

In vivo ubiquitination assay

For in vivo ubiquitination assay, C4-2 cells transfected with plasmids for HA-Ub, FLAG-BRD4 and other indicated proteins. Cells were treated with 20 μM MG132 for 8 h before harvested and lysed with lysis buffer (50 mM Tris-HCl, pH 7.5, 150 mM NaCl, 1% NP40, 0.5% sodium deoxycholate, 1 × protease inhibitor cocktail (PIC)). The lysate was subjected to co-immunoprecipitation using anti-FLAG-conjugated agarose beads as described in Co-IP assay.

Quantitative RT-PCR

Total RNA was isolated from transiently transfected cells using the Trizol reagent (Thermo Fisher Scientific), and cDNA was reverse-transcribed using the Superscript RT kit (TOYOBO, Japan) according to the manufacturer's instructions. PCR amplification was performed using the SYBR Green PCR master mix Kit (TOYOBO, Japan). All quantization were normalized to the level of endogenous control GAPDH. The primer sequences for the SYBR green qPCR used are as follows: BRD2-F: 5′-CTACGTAAGAAACCCCGGAAG-3′; BRD2-R: 5′-GCTTTTTCTCCAAAGCCAGTT-3′; BRD3-F: 5′-CCTCAGGGAGATGCTATCCA-3′; BRD3-R: 5′-ATGTCGTGGTAGTCGTGCAG-3′; BRD4-F: 5′-AGCAGCAACAGCAATGTGAG-3′; BRD4-F: 5′-GCTTGCACTTGTCCTCTTCC-3′; RAC1-F: 5′-TGGCTAAGGAGATTGGTGCT-3′; RAC1-R: 5′-GCAAAGCGTACAAAGGTTCC-3′; FDFT1-F: 5′-ACTATGTTGCTGGGCTGGTC-3′; FDFT1-R: 5′-ACCTGCTCCAAACCTCTTGA-3′; DHCR24-F: 5′-CAAAGGAAATGAGGCAGAGC-3′; DHCR24-R: 5′-TGTGGTACAAGGAGCCATCA-3′; DHCR7-F: 5′-TGACATCTGCCATGACCACT-3′; DHCR7-R: 5′-ACAGGTCCTTCTGGTGGTTG-3′; MVD-F: 5′-AGGACAGCAACCAGTTCCAC-3′; MVD-R: 5′-CACACAGCAGCCACAAACTC-3′; PSA-F: 5′-GGCAGCATTGAACCAGAGGAG-3′; PSA-R: 5′-GCATGAACTTGGTCACCTTCTG-3′; TMPRSS2-F: 5′-CCTGCAAGGACATGGGTAT-3′; TMPRSS2-R: 5′-CGGCACTTGTGTTCAGTTTC-3′; MYC-F: 5′-GGATTCTCTGCTCTCCTC-3′; MYC-R: 5′-CTTGTTCCTCCTCAGAGTC-3′; AR-F: 5′-GACGCTTCTACCAGCTCACC-3′; AR-R: 5′-GCTTCACTGGGTGTGGAAAT-3′; GAPDH-F: 5′-TGCACCACCAACTGCTTAGC-3′; GAPDH-R: 5′-GGCATGGACTGTGGTCATGAG-3′.

Cell proliferation assay

CellTiter 96® AQueous One Solution Cell Proliferation Assay (MTS) (Promega) was used to measure cell growth according to manufacturer's instructions. Briefly, cells were plated in 96-well plates at a density of 2,000 cells per well. At the indicated times, 20 μl of Cell Titer 96R Aqueous One Solution Reagent was added to medium. After incubating for 1 h at 37°C in the cell incubator, cell growth was measured in a microplate reader at 490 nm.

Trypan blue assay

Trypan blue assay was performed to measure cell growth according to manufacturer's instructions. Briefly, cells were plated in 6-well plates at a density of 5×10^4 ~ 1×10^5 cells per well. At the indicated time points, cells were trypsinized and suspended in 1 mL 1×PBS. 100 μL cells and 100 μL trypan blue solution (Sigma-Aldrich) were mixed and the number of viable cells was measured using the Bio-Rad automated cell counter.

Immunohistochemistry (IHC)

FFPE tumor samples from patients or C4-2 xenograft tumors were deparaffinized, rehydrated, and subjected to heat-mediated antigen retrieval. UltraSensitive ™ S-P (Rabbit) IHC Kit (KIT-9706, Fuzhou Maixin Biotech) was used by following the manufacturer's instructions with minor modification as reported previously[37]. Briefly, the sections were incubated with 3% H_2O_2 for 15 min at room temperature to quench endogenous peroxidase activity. After antigen retrieval using unmasking solution (Vector Labs), slides were blocked with normal goat serum for 1 h and then incubated with primary antibody at 4°C overnight. IHC analysis of tumor samples was performed using primary antibodies against BRD2 (dilution 1:250; Abcam; catalog number: ab139690), BRD3 (dilution 1:200; Bethyl; catalog number: A302-368A), and BRD4 (dilution 1:500; Bethyl; catalog number: A301-985A100). The sections were then washed 3 times in 1 × PBS and treated for 30 min with biotinylated goat-anti-rabbit IgG secondary antibodies (Fuzhou Maixin Biotech). After washing three times in 1 × PBS, sections were incubated with streptavidin-conjugated HRP (Fuzhou Maixin Biotech). After washing three times in 1 × PBS for 5 min each, specific detection was developed with 3′3-diaminobenzidine (DAB-2031, Fuzhou Maixin Biotech). Images were taken by using an Olympus camera and matched software. The IHC staining was scored by two independent pathologists based on the 'most common' criteria.

RNA extraction from FFPE patient tissues and RT-qPCR

These experiments were performed using the method described previously[38–40]. Briefly, a 4-μm pre-cut H&E stained section was obtained and reviewed by a pathologist. Only blocks with ≥ 80% tumor cells were used. Total RNA was isolated from FFPE tissue sections from the same cohorts of patients using the RNeasy FFPE Kit (Qiagen, Catalog no. 73504) using the method as reported previously[41]. The NanoDrop 2000 spectrophotometer (Thermo Fisher Scientific) was used to assess the RNA yield and quality. The cDNA was synthesized using PrimeScript™RT reagent Kit (Perfect Real Time) according to the Manufacturer's instruction (TaKaRa, Catalog no. RR037A) with minor modifications. qPCR was performed using SYBR®Premix Ex Taq™II (Tli RNaseH Plus) (TaKaRa, Catalog no. RR820A) on a StepOnePlus Real-Time PCR system (Thermo Fisher Scientific) according to TaKaRa's recommended cycling conditions (95 °C for 30s, followed by 40 cycles of 95 °C for 5 s, 60 °C for 30 s and a melt curve analysis). 18S RNA served as internal reference as reported previously[42]. The primers used in RT-qPCR were listed in Extended Data Table 6. All the samples were run in triplicate on the same plate and the expression level of BRD2/3/4 mRNA was automatically calculated by the StepOnePlus Real-Time PCR system (Thermo Fisher Scientific). The comparison of the expression level of BRD2/3/4 mRNA was performed with Mann-Whitney test by the MedCalc statistical software Version 10.4.7.0

(MedCalc Software bvba, Mariakerke, Belgium). Two-sided $P < 0.05$ was considered statistically significant.

RNA-seq and data analysis

C4-2 cells infected with lentivirus expressing empty vector (EV), HA-SPOP-F133V or BRD2/3/4 were treated with or without JQ1 (1 μM) for 24 h. Total RNAs were isolated from cells using the methods as described previously[43]. Briefly, RNA was isolated using RNeasy Plus Mini Kit (Qiagen). High quality (Agilent Bioanalyzer RIN >7.0) total RNAs were employed for the preparation of sequencing libraries using Illumina TruSeq Stranded Total RNA/Ribo-Zero Sample Prep Kit. A total of 500–1,000 ng of riboRNA-depleted total RNA was fragmented by RNase III treatment at 37°C for 10–18 min and RNase III was inactivated at 65°C for 10 min. Size selection (50 to 150 bp fragments) was performed using the FlashPAGE denaturing PAGE-fractionator (Thermo Fisher Scientific) prior to ethanol precipitation overnight. The resulting RNA was directionally ligated, reverse-transcribed and RNase H treated.

Samples with biological triplicates were sequenced using the Illumina HiSeq2000 platform at the Mayo Clinic Medical Genome Facility. Pre-analysis quality control was performed using FastQC (http://www.bioinformatics.babraham.ac.uk/projects/fastqc/) and RSeQC software[44] to ensure that raw data are in excellent condition and suitable for downstream analyses. Pair-end raw reads were aligned to the human reference genome (GRch37/hg19) using Tophat[45]. Genome-wide coverage signals were represented in BigWig format to facilitate convenient visualization using the UCSC genome browser. Gene expression was measured using RPKM (Reads Per Kilo-base exon per Million mapped reads) as described previously[46]. EdgeR[47] was used to identify genes that were differentially expressed between EV-expressing and SPOP-F133V-expressing C4-2 cells treated with or without JQ1. Raw and processed data have been deposited into NCBI Gene Expression Omnibus with accession number GSE88872.

Chromatin immunoprecipitation (ChIP) sequencing (ChIP-seq) and data analysis, and ChIP-qPCR

ChIP was performed as described previously[48]. ChIP-seq libraries were prepared using the methods as described previously[48] and high throughput sequencing was performed using the Illumina HiSeq2000 platforms at the Mayo Clinic Medical Genome Facility. The data were analyzed using the following pipeline: ChIP-seq raw reads were aligned to the human reference genome (GRCh37/hg19) using Bowtie2 (2.2.9), and reads mapped to one or two locations were kept for further analysis, peak calling was performed by MACS2 (2.1.1) with p-value threshold of 1e-5. BigWig files were generated for visualization with the UCSC genome browser or IGV. We used GREAT (http://bejerano.stanford.edu/great/public/html/) to assign peaks to their potential target genes (a peak-gene association is determined if the peak falls into 2 kb region centering on the transcription start site of the gene). The common BRD4 target genes induced by SPOP F133V and HA-BRD4 expression were determined independently in each of two biological repeat experiments. Raw and processed data have been deposited into NCBI Gene Expression Omnibus with accession number GSE88872.

For ChIP-qPCR experiments, DNAs pulled down by antibodies or non-specific IgG were amplified by real-time PCR. The ChIP primers used were: RAC1 ChIP-F: 5′-CCAAAGTGTTGGGATTACGG-3′; RAC1 ChIP-R: 5′-CGGAGTTTCTCTGGACTTCG-3′; FDFT1 ChIP-F: 5′-ACATCACATGAAGGCCGTTT-3′; FDFT1 ChIP-R: 5′-GACCTTCCACCAACCACCTA-3′. DHCR24 ChIP-F: 5′-CCCTGAGTCAGTCACCCTTT-3′; DHCR24 ChIP-R: 5′-ACAATGGAGCTCACCACTCC-3′; DHCR7 ChIP-F: 5′-GCACATTGATGGAGCGTATG-3′; DHCR7 ChIP-R: 5′-TAATAAGCAGGCCACCCAGA-3′; MVD ChIP-F: 5′-CGCATTACCTCTCAGCCAAT-3′; MVD ChIP-R: 5′-AGACAGGTAGCCCCCACAG-3′; PSA promoter ChIP-F: 5′-CCCTCCCCTTCCACAGC-3′; PSA promoter ChIP-R: 5′-GCCCTATAAAACCTTCATTCCCCAGG-3′. TMPRSS2 ChIP-F: 5′-CGCCCCAGAGTCCCTTAT-3′; TMPRSS2 ChIP-R: 5′-TAATCTCAGGAGGCGGTGTC-3′; MYC ChIP-F: 5′-AGGGATCGCGCTGAGTATAA-3′; MYC ChIP-R: 5′-TGCCTCTCGCTGGAATTACT-3′; AR ChIP-F: 5′-GCAGGAGCTATTCAGGAAGC-3′; AR ChIP-R: 5′-AGGTGGAGAGCAAATGCAAC-3′. Detailed information regarding PCR primers at the enhancer and promoters of all analyzed genes are also summarized in Extended Data Table 6.

Meta-analysis of publically available BRD4 and histone mark ChIP-seq data

BRD4 ChIP-seq data in HEK293T and HeLa cells (accession number GSE51633)[49], H2171 and U87 cells (accession number GSE44931)[50] and mouse acute myeloid leukemia (AML) cells (accession number GSE66122)[51] as well as H3K4me1 and H3K4me3 ChIP-seq data in LNCaP cells[52] were downloaded from NCBI Gene Expression Omnibus. If the original alignments were based on hg18/GRCh36, they were converted into hg19/GRCh37 based-alignments using CrossMap[53]. Peak calling were performed using MACS2 (v2.0.10)[54].

Analysis of JQ1-resistant gene expression in the TCGA dataset and pathway analysis

Primary tumor samples from the prostate cancer cohort in TCGA have been classified into SPOP-MUT (with mutation, N = 48) and SPOP-WT (without mutation, N = 449) groups according to the mutation status of SPOP. Differential expression between the above two groups for the JQ1-resistant genes (n = 1,017) were investigated by Mann–Whitney test with the significance threshold of *P*-value < 0.001. A total of 129 genes have been identified as up-regulated in SPOP-MUT samples. The heat-map was generated using the z-score transformed expression of each gene across all samples. Pathway analyses were performed using Ingenuity IPA.

Cholesterol analysis

The cells were washed with PBS with twice and lysed in the buffer (10 mM Tris-HCl (pH7.6), 500 mM NaCl, 1% Triton X-100, 10 mM β-Methylphenethylamine, 2 mM Na_3VO_4 and 1 mM PMSF) for 30 min on ice. The lysates were extracted in the chloroform/methanol/HCl as described previously[55]. The cholesterol concentration was measured using the Infinity reagent (Thermo Fisher Scientific).

Generation and treatment of prostate cancer xenografts in mice

6-week-old NOD-SCID IL-2-receptor gamma null (NSG) mice were generated in house and randomly divided into different experimental groups as indicated. The animal study was approved by the IACUC at Mayo Clinic. All mice were housed in standard conditions with a 12 h light/dark cycle and access to food and water ad libitum. For BRD2/3/4 knockdown studies, C4-2 cells (5×10^6), infected with lentivirus expressing empty vector (EV) or HA-SPOP-F133V mutant in combination with control shRNA or BRD2/3/4-specific, were mixed with Matrigel (in 100 μl 1×PBS plus 100 μl Matrigel (BD Biosciences)) and injected s.c. into the right flank of mice. After xenografts reached the size of approximately 100 mm^3, vehicle (10% beta cyclodextrin) or JQ1 (Sigma-Aldrich) at 50 mg/kg body weight was administered by i.p. injection 5 days a week. For studies with tumors treated with JQ1 and AKT inhibitor GDC-0068, C4-2 cells (5×10^6) infected with lentivirus expressing empty vector (EV) or HA-SPOP-F133V mutant were mixed with Matrigel (in 100 μl 1×PBS plus 100 μl Matrigel (BD Biosciences)) and injected s.c. into the right flank of mice. After xenografts reached the size of approximately 100 mm^3, vehicle (10% beta cyclodextrin), JQ1 (50 mg/kg) or GDC-0068 (100 mg/kg) were administrated individually or in combination 5 days a week. Growth in tumor volume was measured in a blinded fashion using digital caliper and tumor volumes were estimated using the formula $(L\times W^2)/2$, where L is length of tumor and W is width. The volumes of tumors were compared and P values were determined by a two-tailed Student's t test. Upon the completion of treatment, tumor grafts were harvested. Tumor tissues were divided, and a portion was subjected to FFPE and the rest was frozen for protein and RNA extraction.

Statistical analysis

All data are shown as mean values ± SD for experiments performed with at least three replicates. The difference between 2 groups was analyzed using paired Student's t-test unless otherwise specified. A P value less than 0.05 is considered statistically significant.

Data-availability statement

RNA-seq and ChIP-seq data are available at the NCBI's GEO data repository with the accession code GSE88872. Source data for the uncropped western blots along with molecular weight standards are included in Supplementary Information.

Supplementary Material

Refer to Web version on PubMed Central for supplementary material.

Acknowledgments

This work was supported in part by grants from NIH (CA134514, CA130908 and CA193239 to H.H.) and the Department of Defense (W81XWH-09-1-622 to H. Huang), National Natural Science Foundation of China (81672558, 81201533 to C. Wang; 81572768 to P. Zhang; 31560320 to D. Wang; 31400753 to K. Gao), and National Key Research and Development Plan of China-Precision Medicine Project (2016YFC0902202 to Y. Sun, C. Wang and S. Ren).

References

1. Filippakopoulos P, et al. Selective inhibition of BET bromodomains. Nature. 2010; 468:1067–1073. [PubMed: 20871596]
2. Nicodeme E, et al. Suppression of inflammation by a synthetic histone mimic. Nature. 2010; 468:1119–1123. [PubMed: 21068722]
3. Delmore JE, et al. BET bromodomain inhibition as a therapeutic strategy to target c-Myc. Cell. 2011; 146:904–917. [PubMed: 21889194]
4. Dawson MA, et al. Inhibition of BET recruitment to chromatin as an effective treatment for MLL-fusion leukaemia. Nature. 2011; 478:529–533. [PubMed: 21964340]
5. Zuber J, et al. RNAi screen identifies Brd4 as a therapeutic target in acute myeloid leukaemia. Nature. 2011; 478:524–528. [PubMed: 21814200]
6. Asangani IA, et al. Therapeutic targeting of BET bromodomain proteins in castration-resistant prostate cancer. Nature. 2014; 510:278–282. [PubMed: 24759320]
7. Fong CY, et al. BET inhibitor resistance emerges from leukaemia stem cells. Nature. 2015; 525:538–542. [PubMed: 26367796]
8. Rathert P, et al. Transcriptional plasticity promotes primary and acquired resistance to BET inhibition. Nature. 2015; 525:543–547. [PubMed: 26367798]
9. Shu S, et al. Response and resistance to BET bromodomain inhibitors in triple-negative breast cancer. Nature. 2016; 529:413–417. [PubMed: 26735014]
10. Barbieri CE, et al. Exome sequencing identifies recurrent SPOP, FOXA1 and MED12 mutations in prostate cancer. Nat Genet. 2012; 44:685–689. [PubMed: 22610119]
11. The Molecular Taxonomy of Primary Prostate Cancer. Cell. 2015; 163:1011–1025. [PubMed: 26544944]
12. Theurillat JP, et al. Prostate cancer. Ubiquitylome analysis identifies dysregulation of effector substrates in SPOP-mutant prostate cancer. Science. 2014; 346:85–89. [PubMed: 25278611]
13. Geng C, et al. Prostate cancer-associated mutations in speckle-type POZ protein (SPOP) regulate steroid receptor coactivator 3 protein turnover. Proc Natl Acad Sci U S A. 2013; 110:6997–7002. [PubMed: 23559371]
14. An J, et al. Truncated ERG Oncoproteins from TMPRSS2-ERG Fusions Are Resistant to SPOP-Mediated Proteasome Degradation. Mol Cell. 2015; 59:904–916. [PubMed: 26344096]
15. Zhuang M, et al. Structures of SPOP-substrate complexes: insights into molecular architectures of BTB-Cul3 ubiquitin ligases. Mol Cell. 2009; 36:39–50. [PubMed: 19818708]
16. Blattner M, et al. SPOP Mutations in Prostate Cancer across Demographically Diverse Patient Cohorts. Neoplasia. 2014; 16:14–20. [PubMed: 24563616]
17. Mertz JA, et al. Targeting MYC dependence in cancer by inhibiting BET bromodomains. Proc Natl Acad Sci U S A. 2011; 108:16669–16674. [PubMed: 21949397]
18. Loven J, et al. Selective inhibition of tumor oncogenes by disruption of super-enhancers. Cell. 2013; 153:320–334. [PubMed: 23582323]
19. Roe JS, Mercan F, Rivera K, Pappin DJ, Vakoc CR. BET Bromodomain Inhibition Suppresses the Function of Hematopoietic Transcription Factors in Acute Myeloid Leukemia. Mol Cell. 2015; 58:1028–1039. [PubMed: 25982114]
20. Lu J, et al. Hijacking the E3 Ubiquitin Ligase Cereblon to Efficiently Target BRD4. Chem Biol. 2015; 22:755–763. [PubMed: 26051217]
21. Zhuang L, Lin J, Lu ML, Solomon KR, Freeman MR. Cholesterol-rich lipid rafts mediate akt-regulated survival in prostate cancer cells. Cancer Res. 2002; 62:2227–2231. [PubMed: 11956073]
22. Yue S, et al. Cholesteryl ester accumulation induced by PTEN loss and PI3K/AKT activation underlies human prostate cancer aggressiveness. Cell Metab. 2014; 19:393–406. [PubMed: 24606897]
23. Lasserre R, et al. Raft nanodomains contribute to Akt/PKB plasma membrane recruitment and activation. Nat Chem Biol. 2008; 4:538–547. [PubMed: 18641634]
24. Saci A, Cantley LC, Carpenter CL. Rac1 regulates the activity of mTORC1 and mTORC2 and controls cellular size. Mol Cell. 2011; 42:50–61. [PubMed: 21474067]

25. Esen E, et al. WNT-LRP5 signaling induces Warburg effect through mTORC2 activation during osteoblast differentiation. Cell Metab. 2013; 17:745–755. [PubMed: 23623748]
26. Blattner M, et al. SPOP Mutation Drives Prostate Tumorigenesis In Vivo through Coordinate Regulation of PI3K/mTOR and AR Signaling. Cancer Cell. 2017; 31:436–451. [PubMed: 28292441]
27. Stratikopoulos EE, et al. Kinase and BET Inhibitors Together Clamp Inhibition of PI3K Signaling and Overcome Resistance to Therapy. Cancer Cell. 2015; 27:837–851. [PubMed: 26058079]
28. Saura C, et al. A First-in-Human Phase I Study of the ATP-Competitive AKT Inhibitor Ipatasertib Demonstrates Robust and Safe Targeting of AKT in Patients with Solid Tumors. Cancer Discov. 2017; 7:102–113. [PubMed: 27872130]
29. An J, Wang C, Deng Y, Yu L, Huang H. Destruction of Full-Length Androgen Receptor by Wild-Type SPOP, but Not Prostate-Cancer-Associated Mutants. Cell Rep. 2014; 6:657–669. [PubMed: 24508459]
30. Groner AC, et al. TRIM24 Is an Oncogenic Transcriptional Activator in Prostate Cancer. Cancer Cell. 2016; 29:846–858. [PubMed: 27238081]
31. Chan SC, et al. Targeting chromatin binding regulation of constitutively active AR variants to overcome prostate cancer resistance to endocrine-based therapies. Nucleic Acids Res. 2015; 43:5880–5897. [PubMed: 25908785]
32. Blee AM, Liu S, Wang L, Huang H. BET bromodomain-mediated interaction between ERG and BRD4 promotes prostate cancer cell invasion. Oncotarget. 2016; 7:38319–38332. [PubMed: 27223260]
33. Wang D, et al. Reprogramming transcription by distinct classes of enhancers functionally defined by eRNA. Nature. 2011; 474:390–394. [PubMed: 21572438]
34. An J, Wang C, Deng Y, Yu L, Huang H. Destruction of Full-Length Androgen Receptor by Wild-Type SPOP, but Not Prostate-Cancer-Associated Mutants. Cell Rep. 2014; 6:657–669. [PubMed: 24508459]
35. Hayward SW, et al. Establishment and characterization of an immortalized but non-transformed human prostate epithelial cell line: BPH-1. In Vitro Cell Dev Biol Anim. 1995; 31:14–24. [PubMed: 7535634]
36. Drost J, et al. Organoid culture systems for prostate epithelial and cancer tissue. Nat Protoc. 2016; 11:347–358. [PubMed: 26797458]
37. Patel AJ, et al. BET bromodomain inhibition triggers apoptosis of NF1-associated malignant peripheral nerve sheath tumors through Bim induction. Cell Rep. 2014; 6:81–92. [PubMed: 24373973]
38. Renwick N, et al. Multicolor microRNA FISH effectively differentiates tumor types. J Clin Invest. 2013; 123:2694–2702. [PubMed: 23728175]
39. An J, et al. Truncated ERG Oncoproteins from TMPRSS2-ERG Fusions Are Resistant to SPOP-Mediated Proteasome Degradation. Mol Cell. 2015; 59:904–916. [PubMed: 26344096]
40. Zhao Y, et al. Activation of P-TEFb by Androgen Receptor-Regulated Enhancer RNAs in Castration-Resistant Prostate Cancer. Cell Rep. 2016; 15:599–610. [PubMed: 27068475]
41. Mittempergher L, et al. Gene expression profiles from formalin fixed paraffin embedded breast cancer tissue are largely comparable to fresh frozen matched tissue. PLoS One. 2011; 6:e17163. [PubMed: 21347257]
42. Hagen RM, Rhodes A, Oxley J, Ladomery MR. A M-MLV reverse transcriptase with reduced RNaseH activity allows greater sensitivity of gene expression detection in formalin fixed and paraffin embedded prostate cancer samples. Exp Mol Pathol. 2013; 95:98–104. [PubMed: 23739432]
43. Wang L, et al. BRCA1 is a negative modulator of the PRC2 complex. Embo J. 2013; 32:1584–1597. [PubMed: 23624935]
44. Wang L, Wang S, Li W. RSeQC: quality control of RNA-seq experiments. Bioinformatics. 2012; 28:2184–2185. [PubMed: 22743226]
45. Trapnell C, Pachter L, Salzberg SL. TopHat: discovering splice junctions with RNA-Seq. Bioinformatics. 2009; 25:1105–1111. [PubMed: 19289445]

46. Mortazavi A, Williams BA, McCue K, Schaeffer L, Wold B. Mapping and quantifying mammalian transcriptomes by RNA-Seq. Nature methods. 2008; 5:621–628. [PubMed: 18516045]
47. Robinson MD, Oshlack A. A scaling normalization method for differential expression analysis of RNA-seq data. Genome Biol. 2010; 11:R25. [PubMed: 20196867]
48. Boyer LA, et al. Core transcriptional regulatory circuitry in human embryonic stem cells. Cell. 2005; 122:947–956. [PubMed: 16153702]
49. Liu W, et al. Brd4 and JMJD6-associated anti-pause enhancers in regulation of transcriptional pause release. Cell. 2013; 155:1581–1595. [PubMed: 24360279]
50. Loven J, et al. Selective inhibition of tumor oncogenes by disruption of super-enhancers. Cell. 2013; 153:320–334. [PubMed: 23582323]
51. Roe JS, Mercan F, Rivera K, Pappin DJ, Vakoc CR. BET Bromodomain Inhibition Suppresses the Function of Hematopoietic Transcription Factors in Acute Myeloid Leukemia. Mol Cell. 2015; 58:1028–1039. [PubMed: 25982114]
52. Wang D, et al. Reprogramming transcription by distinct classes of enhancers functionally defined by eRNA. Nature. 2011; 474:390–394. [PubMed: 21572438]
53. Zhao H, et al. CrossMap: a versatile tool for coordinate conversion between genome assemblies. Bioinformatics. 2014; 30:1006–1007. [PubMed: 24351709]
54. Zhang Y, et al. Model-based analysis of ChIP-Seq (MACS). Genome Biol. 2008; 9:R137. [PubMed: 18798982]
55. Zhuang L, Kim J, Adam RM, Solomon KR, Freeman MR. Cholesterol targeting alters lipid raft composition and cell survival in prostate cancer cells and xenografts. J Clin Invest. 2005; 115:959–968. [PubMed: 15776112]

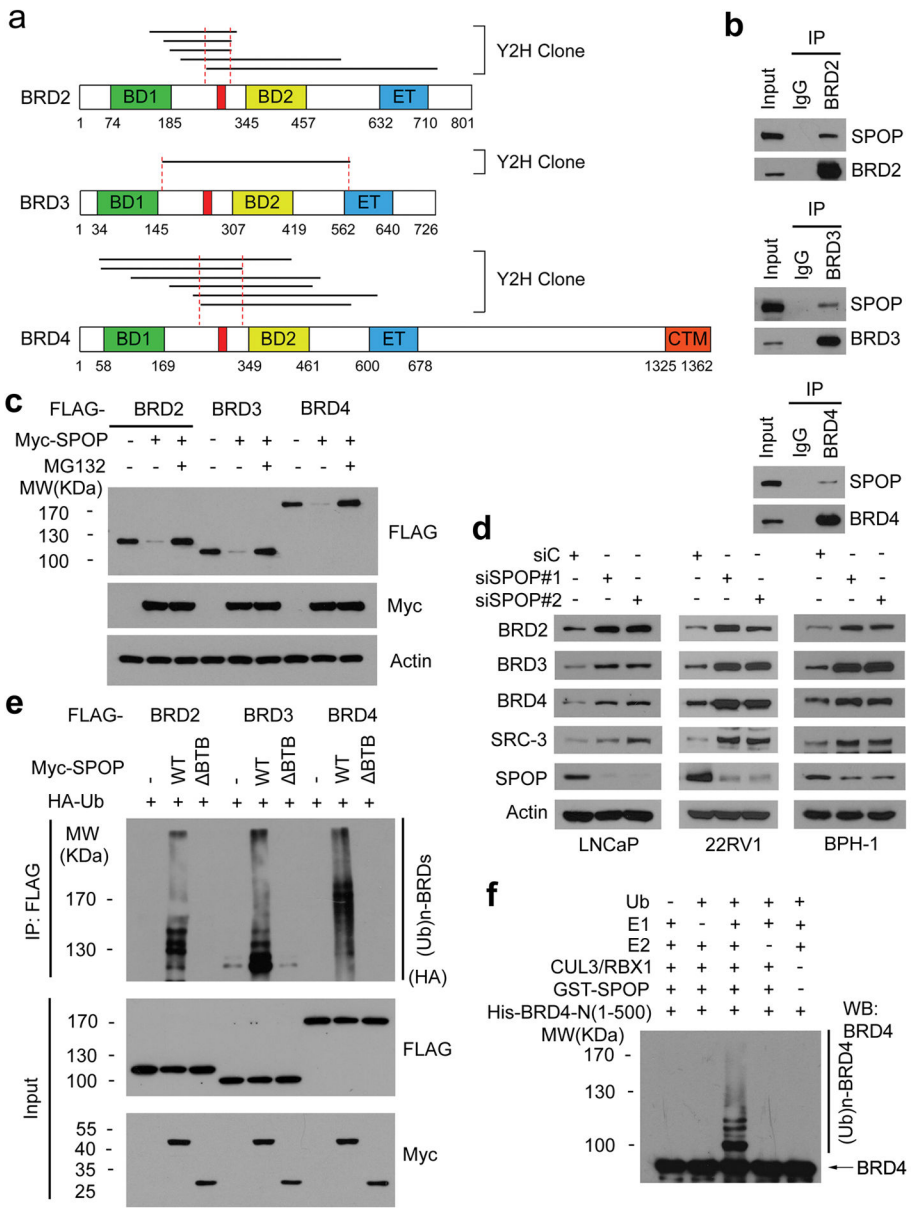

Figure 1. SPOP interacts with and promotes BRD2/3/4 protein ubiquitination and degradation

a, Diagram showing portions of BRD2/3/4 proteins identified by yeast two-hybrid screen in a human fetal brain cDNA library using the full-length SPOP as bait. The region between two dashed red lines is the minimal interaction region shared by positive clones, and the bolded red vertical line represents the SBC motif. BD1, bromodomain 1; BD2, bromodomain 2; ET, extraterminal domain; CTM, C-terminal motif.

b, Western blot of co-IP samples of IgG or anti-BRD2/3/4 antibodies from cell lysate of LNCaP cells treated with 20 μM MG132 for 8 h.

c, Western blot of whole cell lysate (WCL) of 293T cells transfected with indicated plasmids and treated with or without 20 μM MG132 for 8 h. Actin was used as a loading control.

d, Western blot of WCL of different cell lines transfected with indicated siRNAs.

e, Western blot of the products of in vivo ubiquitination assay performed using cell lysate of 293T cells transfected with indicated plasmids and treated with 20 μM MG132 for 8 h.
f, Western blot of the products of in vitro ubiquitination assay performed by incubating the reconstituted SPOP-CUL3-RBX1 E3 ligase complex with E1, E2, Ub, and His-BRD4-N (amino acids 1–500) at 30°C for 2 h.

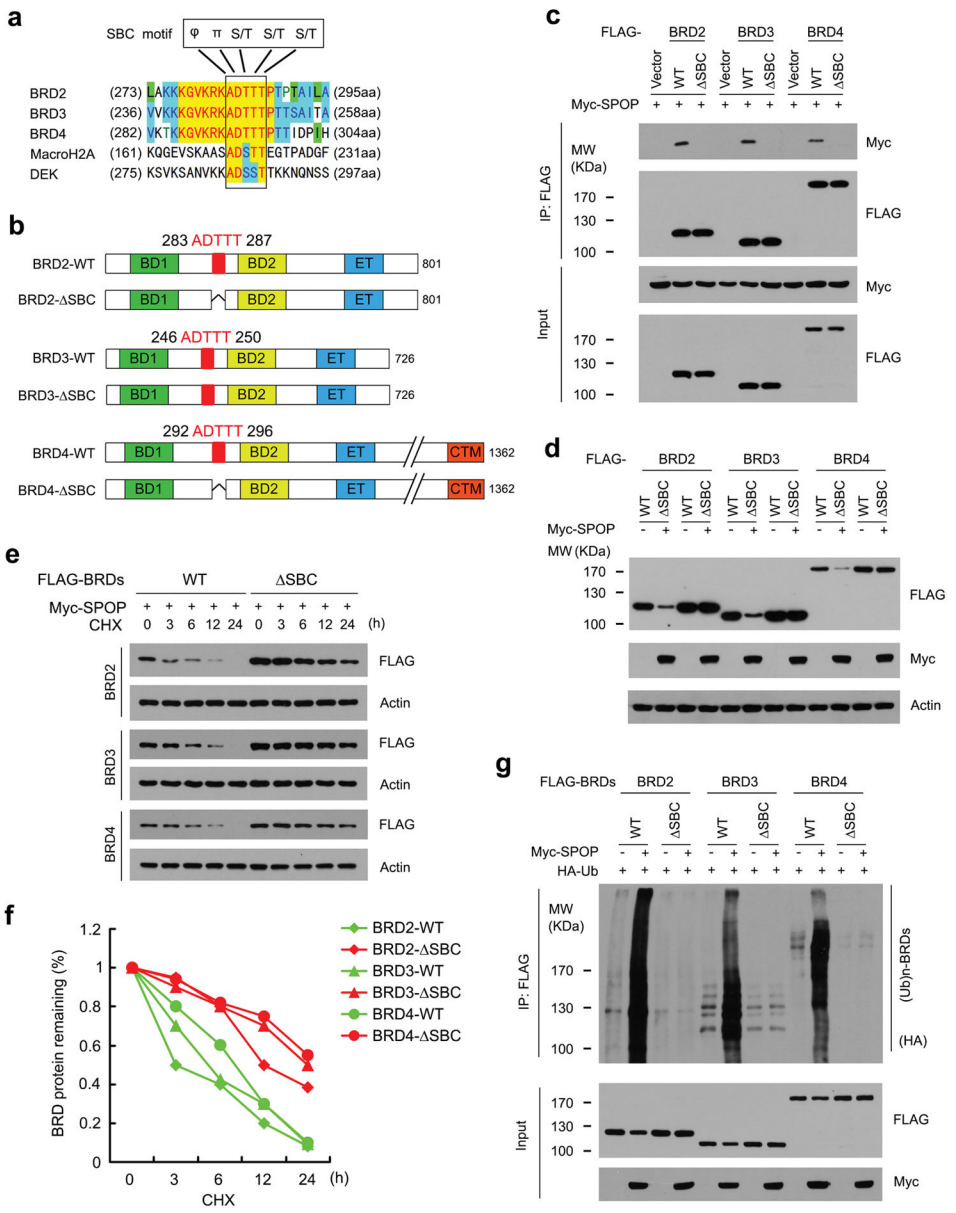

Figure 2. The SBC motif in BRD2/3/4 is a SPOP-recognized degron

a, Amino acid (aa) sequencing alignment of a putative SBC motif in BRD2/3/4. MacroH2A and DEK, positive controls. Φ represents a nonpolar residue and **π** represents a polar residue. S, serine; T, threonine.

b, Diagram showing the wild-type BRD2/3/4 and SBC motif-deleted mutants.

c, Western blot of WCL and co-IP samples of anti-FLAG antibody from 293T cells transfected with indicated plasmids and treated with 20 μM MG132 for 8 h.

d, Western blot of WCL of 293T cells transfected with indicated plasmids.

e and **f**, Western blot of WCL of 293T cells transfected with indicated plasmids and treated with 50 μg/ml cycloheximide (CHX) and harvested at different time points (**e**). At each time point, the intensity of BET protein was normalized to the intensity of actin and then to the value at 0 h (**f**).

g, Western blot of the products of in vivo ubiquitination assay from 293T cells transfected with indicated plasmids and treated with 20 μM MG132 for 8 h.

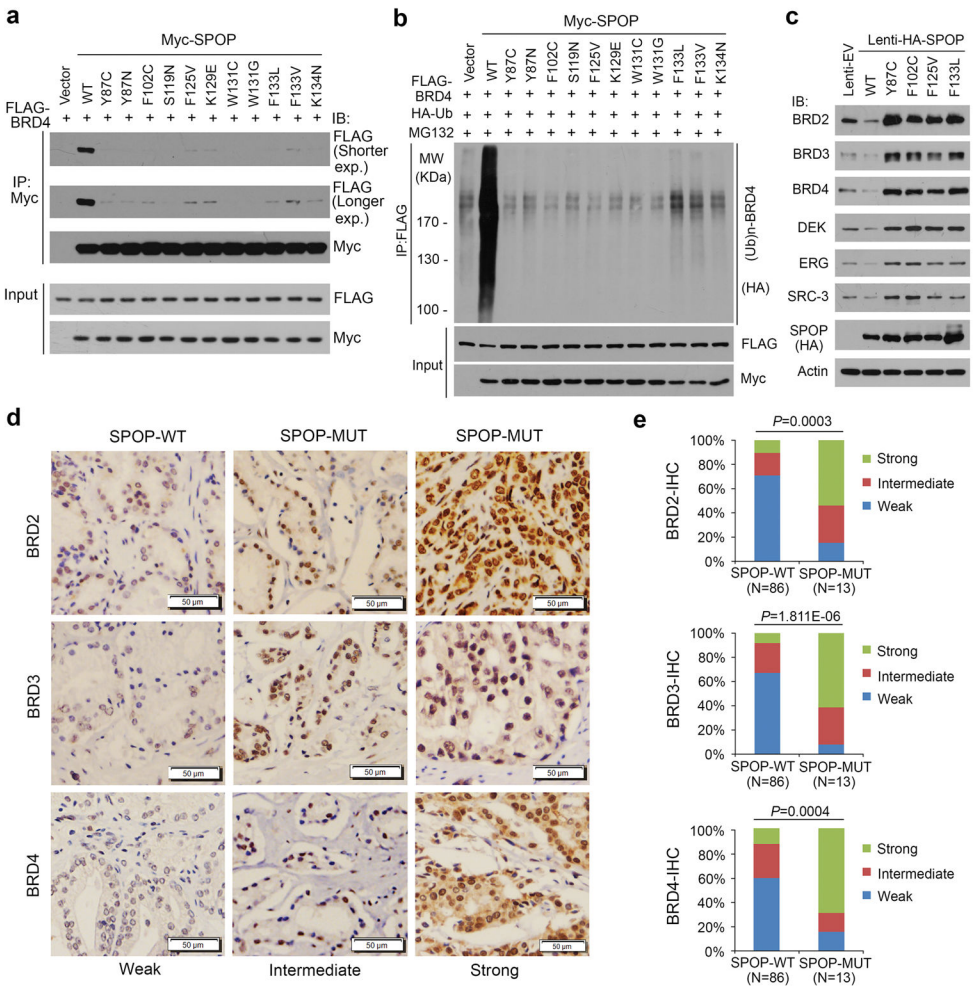

Figure 3. Expression of BET proteins is elevated in SPOP mutant-expressing prostate cancer cells and patient specimens

a, Western blot of WCL and co-IP samples of anti-FLAG antibody from 293T cells transfected with indicated Myc- or FLAG-tagged plasmids and treated with 20 μM MG132 for 8 h.

b, Western blot of the products of *in vivo* ubiquitination assay from 293T cells transfected with indicated Myc- or FLAG-tagged plasmids and treated with 20 μM MG132 for 8 h.

c, Western blot of indicated proteins in WCL of C4-2 cells infected with lentivirus expressing empty vector (EV), wild-type (WT) or mutated SPOP.

d and **e**, Representative images of BRD2/3/4 IHC in SPOP-WT and -mutated (MUT) prostate cancer tissues (**d**). The quantitative data of BRD2/3/4 staining are shown in (**e**). Statistical significance was determined by Wilcoxon rank sum test.

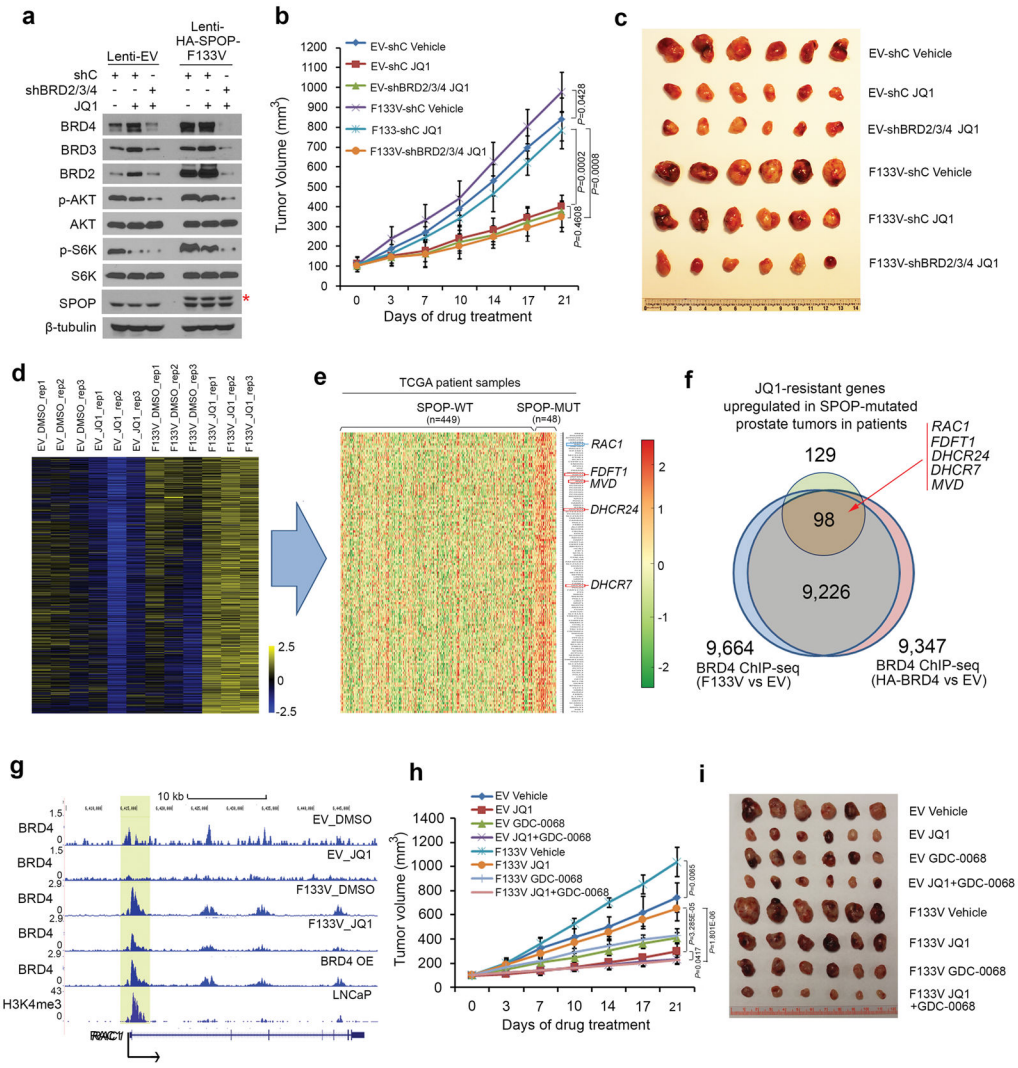

Figure 4. Mechanism of BET inhibitor resistance in SPOP-mutated prostate cancer cells

a, Western blot of indicated proteins including p-AKT (Ser473) and p-S6K (Thr389) in C4-2 cells infected with lentivirus expressing empty vector (EV) or SPOP-F133V mutant in combination with control shRNA (shC) or BRD2/3/4-specific shRNAs. Cells were treated with or without JQ1 (1 μM) for 24 h before harvested. Asterisk in red indicates exogenous SPOP-F133V mutant.

b, C4-2 cells infected with lentivirus as in (**a**) were implanted subcutaneously in mice (n = 6/group). When tumors reached a size of approximately 100 mm^3, xenografted mice were treated with vehicle or JQ1 (50 mg/kg) 5 days a week. Tumors were measured by caliper twice a week. Data are shown as means ± SD. Statistical significance was determined by two-tailed Student's *t*-test for tumors at day 21 of drug treatment.

c, Image of tumors isolated from each group of mice at day 21 of drug treatment as shown in (**b**).

d, Heat map of RNA-seq data shows expression of a cluster of genes (n = 1,017) in C4-2 cells infected with lentivirus expressing EV or F133V and treated with or without JQ1 (1 μM) for 24 h.

e, Heat map showing expression of 129 genes associated with JQ1 resistance was upregulated in SPOP-mutated (MUT) prostate tumors compared to SPOP-WT tumors in the TCGA cohort.

f, Venn diagram shows that JQ1-resistant genes upregulated in SPOP-mutated prostate tumors significantly overlapped with the common BRD4 target genes of SPOP F133V and HA-BRD4 overexpressed (OE) in C4-2 cells (P = 9.407e-12, Permutation test).

g, UCSC genome browser screen shots showing BRD4 ChIP-seq signal profiles in the *RAC1* gene locus in C4-2 cells expressing EV, F133V or HA-BRD4 treated with DMSO or JQ1 (1 μM) for 24 h. H3K4me3 ChIP-seq was acquired from LNCaP cells as reported previously[33].

h, C4-2 cells infected with lentivirus as in (**a**) were implanted subcutaneously in mice (n = 6/group). When tumors reached a size of approximately 100 mm^3, xenografted mice were treated with vehicle, JQ1 (50 mg/kg) or GDC-0068 (100 mg/kg) individually or in combination 5 days a week. Tumors were measured by caliper twice a week. Data are shown as means ± SD. Statistical significance was determined by two-tailed Student's *t*-test for tumors at day 21 of drug treatment.

i, Image of tumors isolated from each group of mice at day 21 of drug treatment as shown in (**h**).